Applied Catalysis B: Environmental 127 (2012) 129–136

Contents lists available at SciVerse ScienceDirect

Applied Catalysis B: Environmental

journal homepage: www.elsevier.com/locate/apcatb

Active size-controlled Ru catalysts for selective CO oxidation in H_2

Yun Ha Kim [a], Jung Eun Park [a], Hyun Chul Lee [b], Sun Hee Choi [c], Eun Duck Park [a,*]

[a] Division of Energy Systems Research and Division of Chemical Engineering and Materials Engineering, Ajou University, Woncheon-Dong Yeongtong-Gu Suwon, 443-749, Republic of Korea
[b] Energy Laboratory, Samsung Advanced Institute of Technology (SAIT), Samsung Electronics, Yongin, Kyunggi-do 446-712, Republic of Korea
[c] Pohang Accelerator Laboratory, Pohang University of Science and Technology (POSTECH), Hyoja-dong, Pohang, 790-784, Republic of Korea

ARTICLE INFO

Article history:
Received 21 October 2011
Received in revised form 20 July 2012
Accepted 13 August 2012
Available online 21 August 2012

Keywords:
Selective CO oxidation
Ru catalysts
Pretreatment
CO oxidation
Size effect

ABSTRACT

We propose an activation method to control Ru particle size in supported Ru catalysts, viz. commercial Ru/Al_2O_3 and home-made Ru/SiO_2, in order to increase the catalytic activity for the preferential CO oxidation (PROX). Ru particle size is controlled by adjusting pre-treatment conditions and it affects the catalytic activity for the PROX over supported Ru catalysts. Several measurements: inductively coupled plasma-atomic emission spectroscopy (ICP-AES), bright-field transmission electron microscopy (TEM), X-ray absorption fine structure (XAFS), CO chemisorption, and O_2 chemisorption were conducted to characterize the catalysts. The co-presence of H_2 and O_2 is essential for controlling the Ru particle size accurately. The PROX activity especially at low temperatures increases with increasing particle size of Ru, which seems to be closely related to the adsorption behavior of O_2 on Ru surface.

1. Introduction

Recently, metal and/or metal oxide nanoparticles with particles ranging from 1 to 20 nm have attracted considerable attention in various fields because of their unique properties [1–6]. The control of the particle size, which in turn changes the surface-to-volume ratio of nanoparticles, is also an important issue in catalysis because all the catalytic reactions occur at the metal and/or metal oxide surface [7,8]. Furthermore, the catalyst performance is sensitive to the particle size of active metal or metal oxides in the catalyst because the surface structure and electronic properties of the nanoparticles can be significantly altered in this size range [7–14]. The formation of nanoparticles in the presence of surface-capping agents and the subsequent anchoring of these particles on a support is a well-known methodology employed in the case of nanocatalysts [9–11]. Moreover, it has been reported that the physical or chemical pre-treatment of the supported metal or metal oxide catalysts can be carried out to control their particle size [12–14].

With the increasing need for a highly efficient energy conversion system, fuel cells have attracted considerable attention, and consequently, there is a need to develop a high-performance fuel processor, in which various hydrocarbons are transformed into H_2. Preferential CO oxidation (PROX) is an essential step in a fuel processing system for a low-temperature polymer electrolyte membrane fuel cell (PEMFC). The purpose of this step is to remove the residual CO in an H_2-rich stream, because CO can degrade the electrochemical performance of the Pt-based anode of PEMFC [15,16]. In the PROX system, CO oxidation ($CO + (1/2)O_2 \rightarrow CO_2$) occurs predominantly, rather than H_2 oxidation ($H_2 + (1/2)O_2 \rightarrow H_2O$). Moreover, two hydrogenation reactions ($CO + 3H_2 \rightarrow CH_4 + H_2O$, $CO_2 + 4H_2 \rightarrow CH_4 + 2H_2O$) and the water-gas shift reaction ($CO + H_2O \rightarrow CO_2 + H_2$) occur because all the reactants (CO, CO_2, H_2, and H_2O) coexist.

While searching for PROX catalysts, some researchers reported the high catalytic activity at low temperatures through the addition of promoters in the case of Pt-based catalysts [17–21]. Nevertheless, Ru-based catalysts have been proposed as active ones because of their excellent performance at low temperatures [22,23]. Besides noble metal catalysts, active studies on non-noble metal PROX catalysts have been underway owing to their low cost [24–28]. Compared to the number of studies on Pt-based catalysts, few studies have been conducted on the improvement of the catalytic performance of Ru-based catalysts [29–43]. Some factors, such as the types of Ru precursors [29,30], pre-treatment conditions [29–32] and types of supports [30,31,33–35] were examined in terms of their effect on the PROX activity. However, thus far, no detailed study has been carried out to examine the effect of the Ru particle size on the PROX activity.

Herein we propose an activation method for controlling the Ru particle size in order to increase the catalytic activity of Ru catalysts in PROX. In the case of supported Ru catalysts, the Ru particle size is controlled by changing the composition of the pre-treatment

* Corresponding author. Tel.: +82 31 219 2384; fax: +82 31 219 1612.
E-mail address: edpark@ajou.ac.kr (E.D. Park).

0926-3373/$ – see front matter © 2012 Elsevier B.V. All rights reserved.
http://dx.doi.org/10.1016/j.apcatb.2012.08.010

gas mixture, and the catalytic activity in PROX can be significantly improved by using activated Ru-based catalysts.

2. Experimental

2.1. Catalyst preparation

Ru/Al_2O_3 catalysts were purchased from Aldrich. The Ru concentration in Ru/Al_2O_3 was 5 wt.%. Silica was prepared by the calcination of silica gel (Sigma–Aldrich) at 773 K in air and utilized as a support. Ru/SiO_2 catalysts were prepared by the incipient wetness impregnation method. The Ru concentration in Ru/SiO_2 was determined to be 1.08 wt.%. Ruthenium nitrosylnitrate ($Ru(NO)(NO_3)_3{\cdot}xH_2O$, Aldrich) was utilized as a Ru precursor. Reduced Ru/Al_2O_3 (denoted as $Ru/Al_2O_3(R)$) and Ru/SiO_2 (denoted as $Ru/SiO_2(R)$) were reduced in H_2 at 573 K. Activated Ru/Al_2O_3 (denoted as $Ru/Al_2O_3(A)$) and Ru/SiO_2 (denoted as $Ru/SiO_2(A)$) were prepared by bringing $Ru/Al_2O_3(R)$ and $Ru/SiO_2(R)$ into contact with a reactant gas composed of 1 mol% CO, 1 mol% O_2, 50 mol% H_2, 20 mol% CO_2 and 10 mol% H_2O in He for 1 h at 573 K. Ru/Al_2O_3 catalysts (denoted as $Ru/Al_2O_3(C)$) and Ru/SiO_2 catalysts (denoted as $Ru/SiO_2(C)$) were pre-treated by bringing $Ru/Al_2O_3(R)$ and $Ru/SiO_2(R)$ into contact with a mixed gas of 10 mol% O_2 in He for 1 h at 573 K.

2.2. Catalyst characterization

The Ru content of the prepared Ru/SiO_2 catalysts was analyzed by inductively coupled plasma-atomic emission spectroscopy (ICP-AES, JY 70Plus, Jobin-Yvon).

Bright-field transmission electron microscopy (TEM) images were obtained using a Tecnai G^2 TEM (FEI) operated at 200 kV, and they were used to determine the Ru particle size. The samples were finely ground in a mortar and then dispersed ultrasonically in methanol. Then, they were deposited on a Cu grid covered by a holey carbon film.

The X-ray absorption fine structure (XAFS) spectra were obtained in a transmission mode for the *K*-edge of Ru at beamline 3C1 of the Pohang light source (PAL) operating at 2.5 GeV with a stored current of 150–180 mA. Ar was used as the detector gas for the incident and transmitted beams. In addition to spectra of the catalyst samples, XAFS data were also obtained for Ru foil and RuO_2, which were employed as the Ru references. The data were analyzed using ATHENA software [44].

The pulsed chemisorptions of probe molecules such as CO and O_2 were conducted in an AutoChem 2910 unit (Micromeritics) equipped with a thermal conductivity detector (TCD) to measure consumption of each gas. Quartz U-tube reactors were generally loaded with 0.20 or 0.50 g of samples. All the catalysts were pre-treated by reduction in H_2 at 573 K for 1 h, and then cooled to room temperature. The chemisorptions were carried out at 300 K in 30 mL/min of He stream through a pulsed-chemisorptions technique, in which 500 μl pulses of each gas were utilized. Additionally, the CO chemisorptions of Ru/Al_2O_3 catalysts were conducted at 300 K after exposure to 2 mol% O_2 in He at 300 K for 0.5 h.

2.3. Reactor system and experimental procedure

The catalytic activity measurements were carried out in a small fixed bed reactor with catalysts that were retained between 45- and 80-mesh sieves. To compare the catalytic activities of $Ru/Al_2O_3(A)$ and $Ru/Al_2O_3(R)$, a standard gas composed of 1 mol% CO, 1 mol% O_2, 50 mol% H_2, 20 mol% CO_2 and 5 mol% H_2O in He was brought into contact with 0.10 g of the catalyst without diluents at a flow rate of 100 mL/min (STP) at atmospheric pressure. The steady-state values were obtained at each temperature. The thermocouple was installed just above the catalyst bed to measure the incoming gas temperature.

The kinetic data were obtained by using the differential reactor, where the conversions of CO and O_2 were controlled such that they were less than 15% and the catalysts were diluted with γ-Al_2O_3 to maintain the isothermal condition. To compare the catalytic activities of $Ru/SiO_2(A)$ and $Ru/SiO_2(R)$, a standard gas composed of 1 mol% CO, 1 mol% O_2, 50 mol% H_2, 20 mol% CO_2 and 10 mol% H_2O in He was brought into contact with 0.10 g of the catalyst without diluents at a flow rate of 100 mL/min (STP) at atmospheric pressure. The steady-state values were obtained at each temperature.

Additionally, the stability tests of $Ru/Al_2O_3(R)$ and $Ru/Al_2O_3(A)$ were examined under the differential reactor condition at 350 K with a standard gas of 1 mol% CO, 0.5 mol% O_2, 50 mol% H_2, 20 mol% CO_2 and 10 mol% H_2O in He. Each sample was diluted with γ-Al_2O_3 to maintain the isothermal condition. This catalyst was contacted with a reactant gas at a flow rate of 100 mL (STP)/min at atmospheric pressure.

The effluent from the reactor was analyzed using a gas chromatograph (HP5890A, carbosphere column) to determine the extent of CO and O_2 conversion and CH_4 yield. In all cases, the detection limit for CO was 10 ppm. The extent of CO and O_2 conversion was calculated from the ratio of the consumed amount to the initial amount of each gas. The CH_4 yield was determined from the ratio of the amount of produced CH_4 to the initial amount of CO. The CO conversion, O_2 conversion, and the CH_4 yield were calculated using the following formulas:

$$\text{CO conversion}\,(\%) = \frac{[\text{CO}]_{\text{in}} - [\text{CO}]_{\text{out}}}{[\text{CO}]_{\text{in}}} \times 100;$$

$$\text{O}_2\ \text{conversion}\,(\%) = \frac{[\text{O}_2]_{\text{in}} - [\text{O}_2]_{\text{out}}}{[\text{O}_2]_{\text{in}}} \times 100;$$

$$\text{CH}_4\text{yield}\,(\%) = \frac{[\text{CH}_4]_{\text{out}}}{[\text{CO}]_{\text{in}}} \times 100.$$

3. Results and discussion

To determine the structural and electronic state of Ru/Al_2O_3 catalysts, Ru *k*-edge X-ray absorption near-edge structure (XANES) spectra were obtained. Fig. 1(A) shows the Ru *k*-edge XANES spectra of reduced Ru/Al_2O_3 ($Ru/Al_2O_3(R)$) and activated Ru/Al_2O_3 ($Ru/Al_2O_3(A)$) with Ru references such as Ru foil and RuO_2. The spectra of $Ru/Al_2O_3(R)$ and $Ru/Al_2O_3(A)$ show the presence of Ru metal characterized by two oscillations above the edge jump; moreover, no significant difference is observed between $Ru/Al_2O_3(R)$ and $Ru/Al_2O_3(A)$. The radial structure functions (RSFs) of the Ru foil, $Ru/Al_2O_3(R)$ and $Ru/Al_2O_3(A)$ are shown in Fig. 1(B). In this figure, the main peak corresponds to the Ru-Ru distance (0.240 nm) in the case of the Ru foil; the main peaks of the spectra of $Ru/Al_2O_3(R)$ and $Ru/Al_2O_3(A)$ are also around 0.240 nm. Owing to Ru-Ru interaction, as shown in Table 1, the coordination numbers for $Ru/Al_2O_3(R)$ and $Ru/Al_2O_3(A)$ were 6.5 and 8.2, respectively. This corresponds to 4.3 and 5.9 nm, respectively when assuming spherical Ru nanocrystals [45]. Bright-field TEM images were obtained to determine the Ru particle size of each catalyst, as shown in Fig. 1(C) and (D). The average Ru particle sizes in $Ru/Al_2O_3(R)$ and $Ru/Al_2O_3(A)$ were found to be 4.9 ± 1.5 nm and 6.5 ± 2.2 nm, respectively (Fig. S1). This change in the average Ru particle size after the activation step was also confirmed on the basis of the decrease in the amount of chemisorbed CO and O_2 after the activation, as shown in Table 2. Han et al. [32] reported

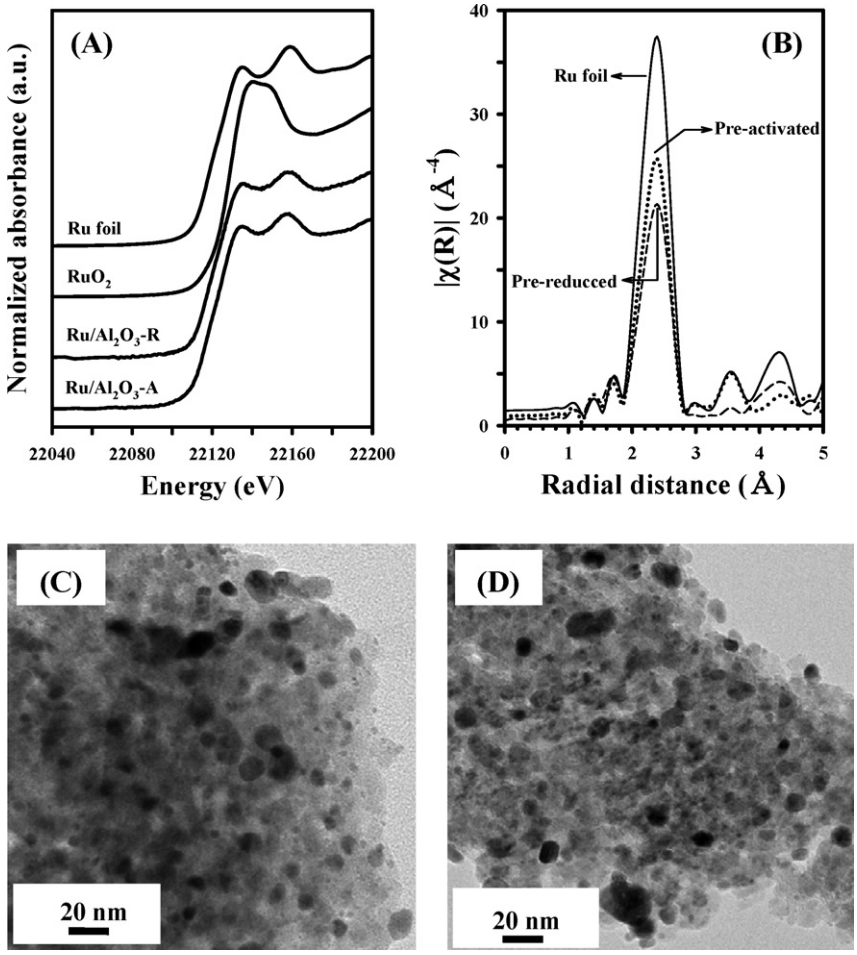

Fig. 1. (A) Ru *k*-edge XANES spectra of Ru foil, RuO_2, Ru/Al_2O_3(R) and Ru/Al_2O_3(A), (B) Fourier-transforms of Ru/Al_2O_3 catalysts, and the bright-field TEM images of (C) Ru/Al_2O_3(R) and (D) Ru/Al_2O_3(A).

an increase in the average Ru particle size through the calcination step.

We prepared calcined Ru/Al_2O_3 (Ru/Al_2O_3(C)) by bringing Ru/Al_2O_3 into contact with 10 mol% O_2 in He for 1 h at 573 K. The average Ru particle size in Ru/Al_2O_3(C) increased significantly, but the particle size distribution was quite broad, as shown in Fig. S2. We also examined the effect of gas composition on Ru particle size during the activation step and found that the presence of O_2 led to the increase in the Ru particle size, whereas H_2 and CO suppressed the extent of the increase in the Ru particle size. On the other hand, CO_2 and H_2O appeared to play a minor role in the activation step. Therefore, the co-presence of the reducing and oxidizing elements is essential for controlling the Ru particle size accurately, as shown in Fig. 2 and Table 3 .

Table 1
The results of EXAFS least-square fits for Ru/Al_2O_3 catalysts.

	Ru/Al_2O_3(R)	Ru/Al_2O_3(A)
CN[a]	6.5	8.2
R (Å)[b]	2.68	2.68
σ^2 (Å^2)[c]	0.0048	0.0051
R-factor[d]	0.0079	0.0016

[a] Coordination number.
[b] Bond distance.
[c] Debye–Waller factor.
[d] Sum-of-squares measure of the fractional misfit.

The catalytic performance of Ru/Al_2O_3(R), Ru/Al_2O_3(A) and Ru/Al_2O_3(C) was examined in the feed stream which was composed of 1.0 mol% CO, 1.0 mol% O_2, 50 mol% H_2, 20 mol% CO_2 and 5 mol% H_2O in He, as shown in Fig. 3. The catalytic activity for CO conversion at low temperatures (below 423 K) decreased in the following order: Ru/Al_2O_3(A) > Ru/Al_2O_3(R) > Ru/Al_2O_3(C). In particular, Ru/Al_2O_3(A) showed the highest catalytic activity for PROX for all ranges of the operating temperature. In the cases of Ru/Al_2O_3(R) and Ru/Al_2O_3(C), the CO conversion decreased steadily with increasing reaction temperature till 453 K but it increased at temperature above 453 K. Generally, it was known that the CO conversion decreased with increasing reaction temperature for the PROX at high temperatures because of the predominant H_2 oxidation. It is worth mentioning that the re-increasing of CO conversion for the PROX over tested all Ru/Al_2O_3 catalysts appeared at high temperature range. This might be due to the water-gas shift reaction ($CO + H_2O \leftrightarrow CO_2 + H_2$) and CO methanation ($CO + 3H_2 \leftrightarrow CH_4 + H_2O$). In the case of supported Ru catalysts, CO methanation occurring simultaneously with PROX was reported to be beneficial for CO removal especially at high temperatures [42]. This can be quite effective as long as CO_2 methanation ($CO_2 + 4H_2 \leftrightarrow CH_4 + 2H_2O$), which consumes excessively large amounts of H_2, does not occur predominantly. It is worth mentioning that CH_4 yields of Ru/Al_2O_3(A) is much lower than those of Ru/Al_2O_3(R), which implies that the former catalyst consumes much smaller amount of H_2 than the latter one

Table 2
The physicochemical properties of Ru/Al_2O_3 and Ru/SiO_2.

Catalyst	Amount of chemisorbed CO[a] ($\mu mol/g_{cat.}$)	[CO]/[Ru][a]	Amount of chemisorbed O_2[b] ($\mu mol/g_{cat.}$)	$[O_2]/[Ru]$[b]
Ru/Al_2O_3(R)	65.9	0.13	78.6	0.16
Ru/Al_2O_3(A)	27.2	0.06	27.0	0.05
Ru/SiO_2(R)	27.5	0.26	10.2	0.10
Ru/SiO_2(A)	4.6	0.04	0.0	0.0

[a] The CO chemisorptions were measured at 300 K in He.
[b] The O_2 chemisorptions were measured at 300 K in He.

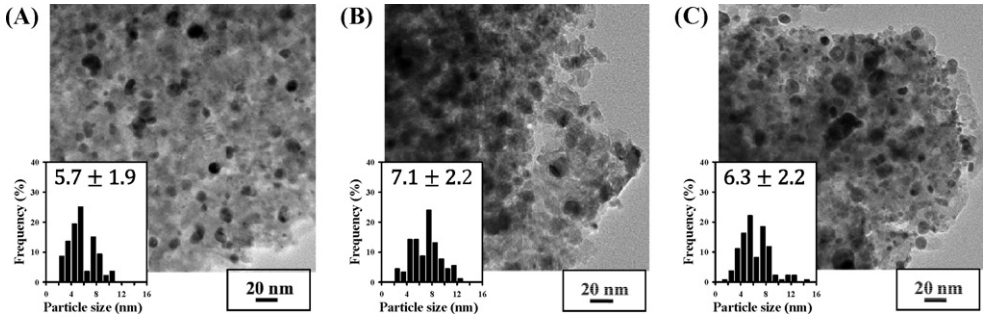

Fig. 2. The bright-field TEM images and particle size distributions of Ru/Al_2O_3 catalysts after pretreatment of mixed gases (1 mol% CO and 50 mol% H_2 in He) at 573 K (A), pretreatment of mixed gases (1 mol% CO and 1 mol% O_2 in He) at 573 K (B), and pretreatment of mixed gases (1 mol% CO, 1 mol% O_2 and 50 mol% H_2 in He) at 573 K (C).

especially at high temperatures. Additionally, the catalytic activity for complete CO oxidation in the absence of H_2 also decreased in the abovementioned order, as shown in Fig. 4. Furthermore, for a fixed catalyst, the CO conversion achieved at a considerably higher temperature in the absence of H_2 was similar to that achieved in the presence of H_2. In the absence of H_2, excess O_2 can be strongly chemisorbed on the Ru surface, and this hinders CO from being chemisorbed on Ru. This chemisorbed O_2 can be removed in the presence of H_2 via H_2 oxidation.

The PROX activity over Ru/Al_2O_3 catalysts pre-treated with different gas composition was also examined in a small fixed bed reactor while increasing the reaction temperatures, as shown in Fig. 5. In this case, all of the catalysts were brought into contact with a He stream after the pre-treatment at 573 K. Compared to Ru/Al_2O_3(R), Ru/Al_2O_3 catalysts pre-treated with a gas stream containing CO and H_2 showed the better PROX activity especially at low temperatures. Especially, Ru/Al_2O_3 catalysts pre-treated with a gas stream containing CO, O_2 and H_2 exhibited the higher CO conversion at all points of temperatures than that pre-treated with a gas stream containing CO and H_2. The former has a larger Ru particle size than the latter, as shown in Fig. 2. On the other hand, the worst PROX activity was obtained at low temperatures over Ru/Al_2O_3 catalysts pre-treated with a gas stream containing CO and O_2 even though it has the largest Ru particle size among tested catalysts in Fig. 5. Since this catalyst was exposed to O_2 during the pre-treatment, the surface oxidation might occur. As a result, it hinders CO from being chemisorbed. This hypothesis is supported by the fact that no detectable amount of chemisorbed CO was obtained at 300 K in Table 3. This result is also consistent with the fact that much higher CO conversion was achieved at a fixed temperature in the presence of H_2 compared with the case in the absence of H_2 over the same catalyst, as shown in Figs. 3 and 4. The importance of the surface oxidation state of Ru on the PROX activity was also confirmed by the fact that the much higher low-temperature PROX activity was obtained over the Ru/Al_2O_3 catalyst pretreated with a hydrogen stream at 573 K before a reaction compared with the case over the Ru/Al_2O_3 catalyst just purged with a He stream after a pre-treatment with a gas stream composed of 1 mol% CO and 1 mol% O_2 in He, as shown in Fig. 5 and Fig. S4. As shown in Table 3, a noticeable amount of CO was chemisorbed for the Ru/Al_2O_3 catalyst pre-treated with a gas stream composed of 1 mol% CO and 1 mol% O_2 in He and then further reduced with a hydrogen stream at 573 K although no detectable amount of CO was chemisorbed for the Ru/Al_2O_3 catalyst just purged with a He stream after a pre-treatment with a gas stream composed of 1 mol% CO and 1 mol% O_2 in He. As shown in Fig. 3 and S4, the Ru/Al_2O_3 catalyst, pre-treated with a gas stream composed of 1 mol% CO and 1 mol% O_2 in He and then further reduced with a hydrogen stream at 573 K, is inferior to Ru/Al_2O_3(A) for the PROX activity. It is worth mentioning that the average particle size of Ru for the former is larger than that for the latter, which implies that there exists an optimum particle size of Ru to show the highest PROX activity. As shown in Table S1 and Figs. S1 and S5, the particle size of Ru can be controlled by adjusting the oxygen content in a pre-treatment gas or the pre-treatment temperature. However, the final particle size of Ru for these catalysts appeared to be larger than that of the Ru/Al_2O_3 catalyst pretreated with a gas stream composed of 1 mol% CO and 1 mol% O_2 in He. Therefore, it can be concluded that the optimum Ru particle size

Table 3
The amount of chemisorbed CO for Ru/Al_2O_3 pretreated at 573 K under different gas compositions.

Catalyst	Gas composition (mol%)	Amount of chemisorbed CO[c] ($\mu mol/g_{cat.}$)	[CO]/[Ru][c]
Ru/Al_2O_3[a]	$CO/H_2/He = 1/50/49$	8.2	0.02
Ru/Al_2O_3[a]	$CO/O_2/He = 1/1/98$	0.0	0.0
Ru/Al_2O_3[a]	$CO/O_2/H_2/He = 1/1/50/48$	13.6	0.03
Ru/Al_2O_3[b]	$CO/O_2/He = 1/1/98$	22.9	0.05

[a] The sample was purged with an He stream at 300 K after the pretreatment.
[b] The sample was reduced with a H_2 stream at 573 K after the pretreatment.
[c] The CO chemisorptions were measured at 300 K in He.

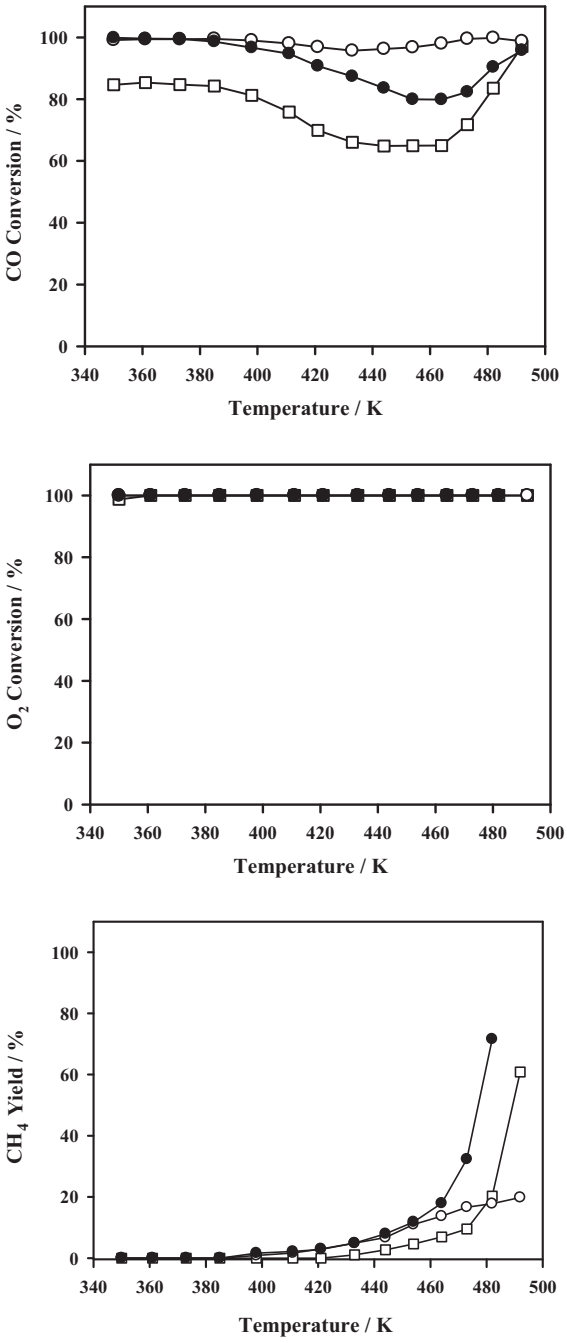

Fig. 3. The steady-state CO conversion, O_2 conversion and CH_4 yield with increasing reaction temperatures for the PROX over Ru/Al_2O_3(R) (●), Ru/Al_2O_3(A) (○) and Ru/Al_2O_3(C) (□). All of the catalysts were reduced with an H_2 stream at 573 K before a reaction. F/W = 1000 mL/min/$g_{cat.}$ Reaction condition: 1 mol% CO, 1 mol% O_2, 50 mol% H_2, 20 mol% CO_2 and 5 mol% H_2O in He.

for the PROX can be made through the pre-treatment with a gas composed of O_2 and H_2.

It is important to mention that the catalytic activity for CO oxidation over Ru catalysts increases with increasing Ru particle size [11,35,46]. This implies that the interaction between O_2 and the Ru surface weakened with increasing Ru particle size. To compare the intrinsic reaction rate of Ru/Al_2O_3(A) with that of Ru/Al_2O_3(R), the turnover frequencies (TOFs), which are normalized by the number of active sites (as measured from the extent of CO chemisorptions), at different temperatures over both the catalysts were obtained by using a differential reactor, as shown

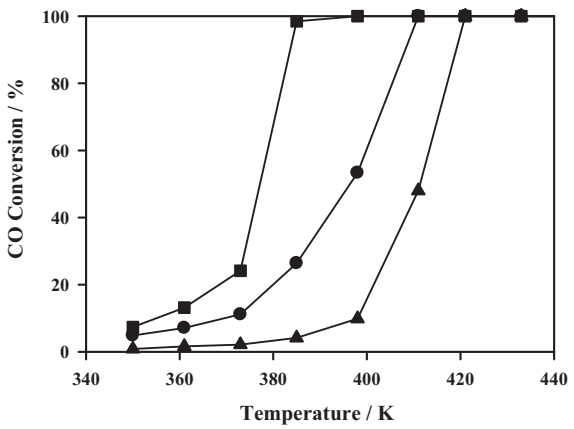

Fig. 4. CO conversion for the complete CO oxidation with increasing reaction temperatures over Ru/Al_2O_3(R) (●), Ru/Al_2O_3(A) (■) and Ru/Al_2O_3(C) (▲). All of the catalysts were reduced with an H_2 stream at 573 K before a reaction. F/W = 1000 mL/min/g_{cat}. Reaction condition: 1 mol% CO and 1 mol% O_2 in He.

in Fig. 6. Ru/Al_2O_3(A) exhibited higher TOFs than Ru/Al_2O_3(R) at all temperatures, but its activation energy was lower than that of Ru/Al_2O_3(R). The activation energies for CO oxidation were determined to be 54.0 kJ/mol and 26.5 kJ/mol for Ru/Al_2O_3(R) and Ru/Al_2O_3(A), respectively. The activation energy for O_2 consumption was determined to be 44.1 kJ/mol and 18.6 kJ/mol for Ru/Al_2O_3(R) and Ru/Al_2O_3(A), respectively. The higher TOF over Ru/Al_2O_3(A) than over Ru/Al_2O_3(R) can be attributed to the larger number of active sites for CO chemisorptions under realistic conditions (gas stream containing CO, O_2, H_2, CO_2 and H_2O). This hypothesis can be supported by the fact that Ru/Al_2O_3(A) possessed a larger number of active sites for CO chemisorption than did Ru/Al_2O_3(R), as determined on the basis of CO chemisorption data after O_2 chemisorption at 300 K in Table 4. Han et al. carried out the kinetic experiment over 5 wt.% Ru/Al_2O_3 under PROX conditions (1 kPa CO, 1 kPa O_2, 65 kPa H_2, 10 kPa H_2O, rest CO_2) and determined the apparent activation energy for the oxidation of CO to be 20 kJ/mol in the low temperature region [40]. They reported that the apparent activation energy was dependent on $[O_2]/[CO]$ ratios and the temperature region.

Additionally, a stability test was conducted over the Ru/Al_2O_3(A) and Ru/Al_2O_3(R) catalysts at 350 K, as shown in Fig. 7. Although the reaction rates decreased slightly at the initial stage, they reached steady-state values and remained constant for 100 h. At all points of time, the specific reaction rate of Ru/Al_2O_3(A) catalyst was found to be significantly higher than that of Ru/Al_2O_3(R). A slow deactivation during PROX over supported Ru catalysts was also reported [36–39], which was tentatively explained by ruthenium oxidation [36–39]. This deactivated catalyst was reported to be reactivated by treatment with hydrogen [36–39]. On the other hand, Han et al. reported that 5 wt.% Ru/Al_2O_3 showed a stable PROX activity at 423 K [40]. As shown in Fig. 5, the Ru/Al_2O_3 catalyst pretreated in oxidizing conditions showed a comparable PROX activity with the Ru/Al_2O_3 catalyst pre-treated in reducing conditions at temperatures above 423 K, which implies that the Ru/Al_2O_3 catalyst pre-treated in oxidizing conditions was reactivated with H_2 in a

Table 4
The CO chemisorption results of Ru/Al_2O_3 catalysts at 300 K after exposure to 2 mol% O_2 in He at 300 K for 0.5 h.

Catalyst	Amount of chemisorbed CO (μmol/$g_{cat.}$)	[CO]/[Ru]
Ru/Al_2O_3(C)	0.0	0.0
Ru/Al_2O_3(R)	10.4	2.1×10^{-2}
Ru/Al_2O_3(A)	14.6	3.0×10^{-2}

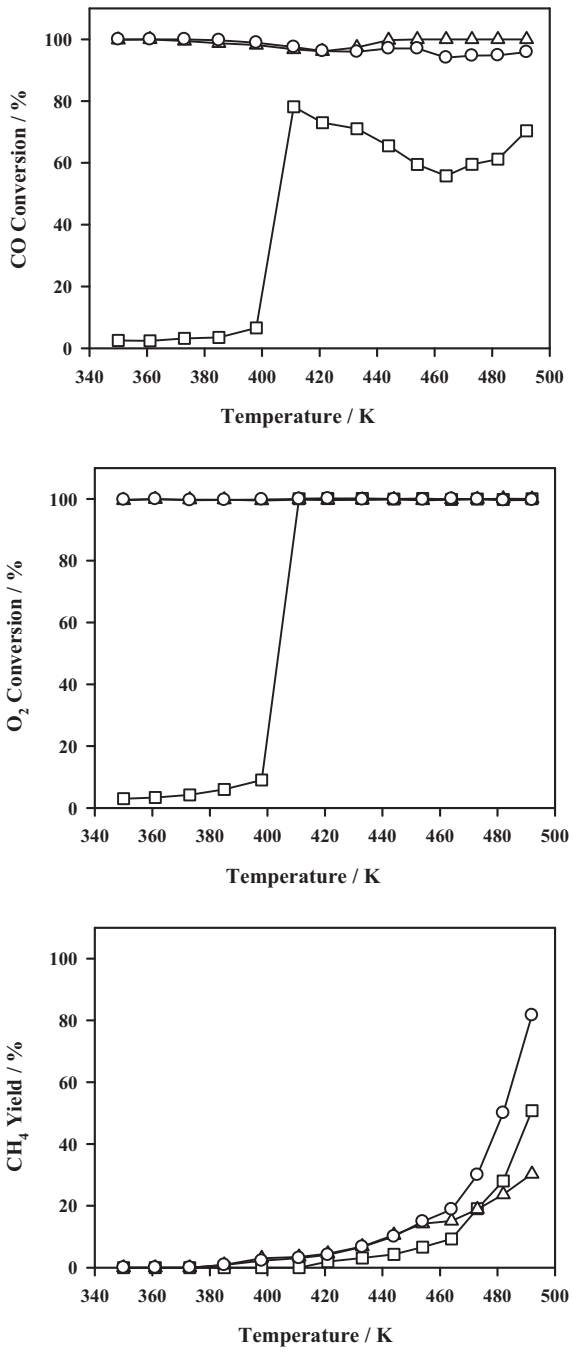

Fig. 5. The steady-state CO conversion, O_2 conversion and CH_4 yield with increasing reaction temperatures for the PROX over supported Ru/Al_2O_3 after pretreatment of mixed gases (1 mol% CO and 50 mol% H_2 in He) (○), pretreatment of mixed gases (1 mol% CO and 1 mol% O_2 in He) (□) and pretreatment of mixed gases (1 mol% CO, 1 mol% O_2 and 50 mol% H_2 in He) (△). Before a reaction, all of the catalysts were brought into contact with a He stream after the pretreatment. F/W = 1000 mL/min/$g_{cat.}$ Reaction condition: 1 mol% CO, 1 mol% O_2, 50 mol% H_2, 20 mol% CO_2 and 5 mol% H_2O in He.

feed. Based on them, it can be said that the strength of O—Ru bond depends on gas composition and temperature, affecting in turn the activity and selectivity and that the slow initial deactivation observed in Fig. 7 could be caused by a transition from the metal to the oxide state. Therefore, it could be mentioned that the metallic Ru nanoparticles with increased particle size in a controlled way in Ru/Al_2O_3(A) catalyst are resistant to further oxidation of active site, resulting in a large amount of active site under working conditions, and finally, exhibit a high catalytic activity for CO oxidation.

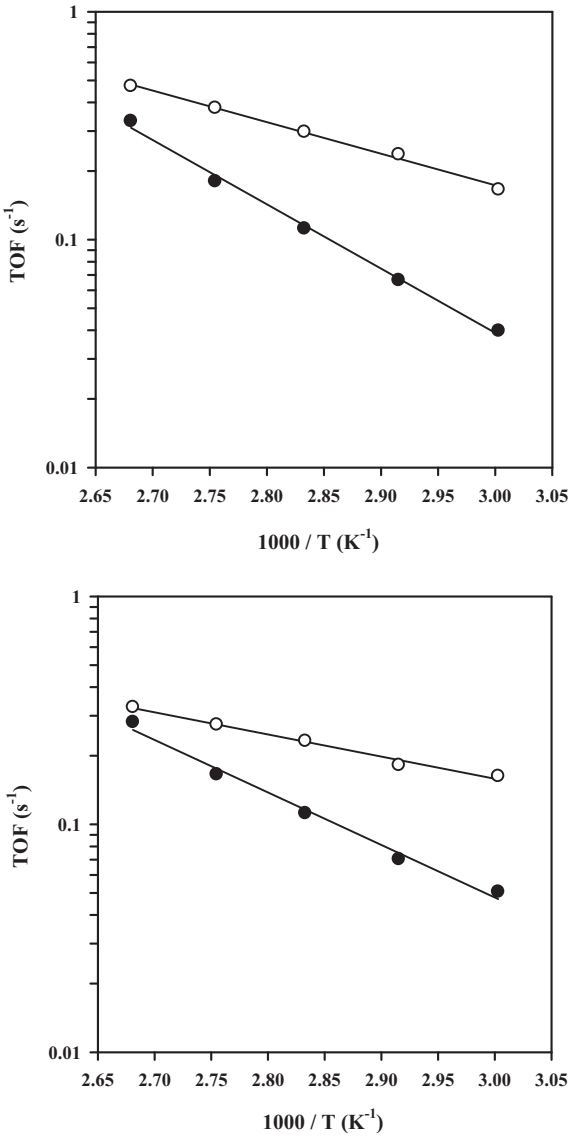

Fig. 6. The turnover frequency (TOF) for CO oxidation (A) and O_2 consumption (B) at different reaction temperatures based on the active sites measured by CO chemisorptions over Ru/Al_2O_3(R) (●) and Ru/Al_2O_3(A) (○). Reaction condition: 1 mol% CO, 1 mol% O_2, 50 mol% H_2, 20 mol% CO_2 and 10 mol% H_2O in He.

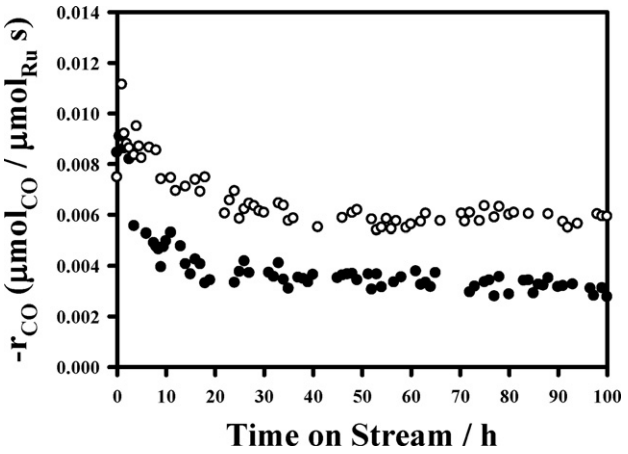

Fig. 7. The specific reaction rate at 350 K based on the Ru content with time on stream for the PROX over Ru/Al_2O_3(R) (●) and Ru/Al_2O_3(A) (○) catalysts. Reaction condition: 1 mol% CO, 0.5 mol% O_2, 50 mol% H_2, 20 mol% CO_2 and 10 mol% H_2O in He.

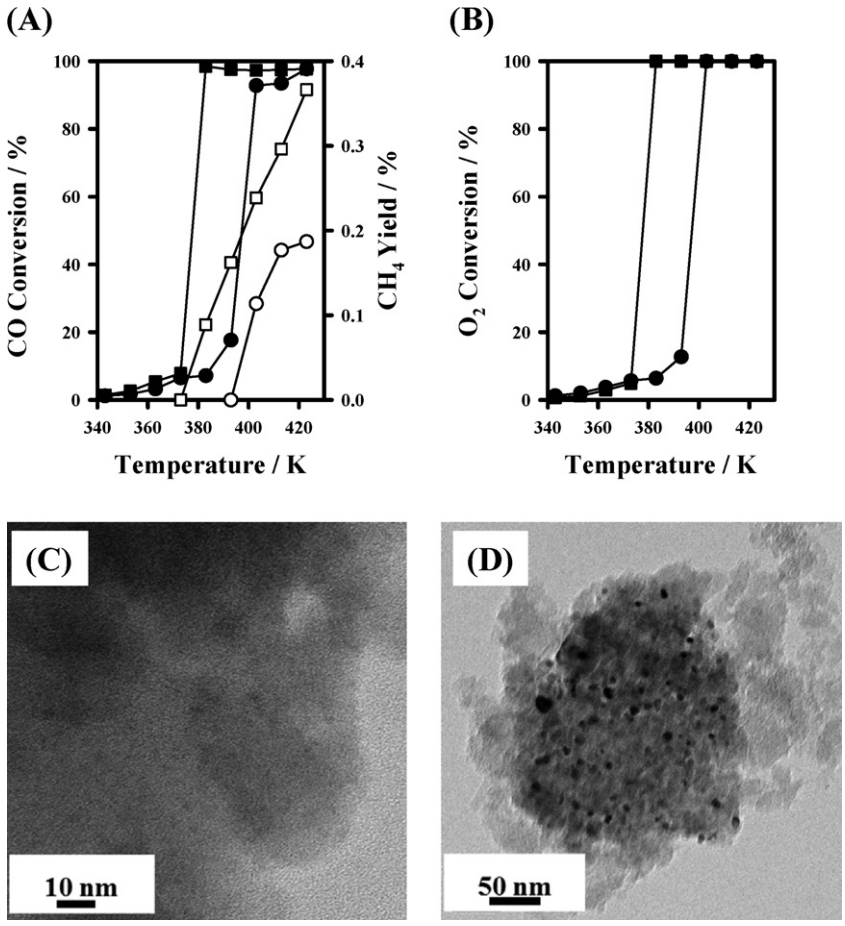

Fig. 8. (A) The CO conversion (filled symbols), CH_4 yield (open symbols) and (B) O_2 conversion with increasing reaction temperatures for the PROX over supported Ru/SiO_2(R) (●, ○) and Ru/SiO_2(A) (■, □) catalysts. F/W = 1000 ml/min/$g_{cat.}$ Reaction condition: 1 mol% CO, 1 mol% O_2, 50 mol% H_2, 20 mol% CO_2 and 10 mol% H_2O in He. The bright-field TEM images of (C) Ru/SiO_2(R) and (D) Ru/SiO_2(A).

We also applied this activation method to Ru catalysts prepared in house, namely, Ru/SiO_2. In this case, we chose a different support, SiO_2, to verify the availability of this activation method for other supported Ru catalysts. As shown in Fig. 8(A), activated Ru/SiO_2 (Ru/SiO_2(A)) showed higher catalytic activity than reduced Ru/SiO_2 (Ru/SiO_2(R)) in PROX at all temperatures. Furthermore, the former also resulted in a higher CH_4 yield than the latter. There was a temperature region, where CO and O_2 conversion increased rapidly, in Fig. 8(A) and (B). This is called ignition caused by a jump in the temperature of the catalyst surface, which is frequently observed in the highly exothermic reaction. In this region, the reaction goes from the kinetic into the external mass transfer control regime. Kipnis and Volnina reported that there existed a temperature discrepancy across the catalyst bed especially at ignition temperature [43]. In this work, the thermocouple was installed just above the catalyst bed. Therefore, there should be a discrepancy between the measured temperature and the real temperature of the catalyst surface. However, the ignition occurred at much lower temperature over Ru/SiO_2(A) than that over Ru/SiO_2(R), which implies that Ru/SiO_2(A) is much superior to Ru/SiO_2(R) for PROX.

A TEM image of each catalyst (Fig. 8(C) and (D)) was obtained to determine the Ru particle size in Ru/SiO_2 catalysts. The average Ru particle sizes in Ru/SiO_2(R) and Ru/SiO_2(A) were determined to be 1.5 ± 0.5 nm and 6.4 ± 2.1 nm, respectively (Fig. S3). For comparison, we also prepared calcined Ru/SiO_2 (Ru/SiO_2(C)) by bringing Ru/SiO_2 into contact with 10 mol% O_2 in He for 1 h at 573 K. The average Ru particle size in Ru/SiO_2(C) increased significantly, but the particle size distribution was quite broad, as shown in Fig. S2. These results also support that the co-presence of the reducing and oxidizing elements is essential for controlling the Ru particle size accurately.

4. Conclusion

In this study, we proposed an activation method to increase the Ru particle size in supported Ru catalysts and used these catalysts for selective CO oxidation in an H_2-rich stream. The activated Ru catalyst showed higher catalytic activity than the fresh catalysts; this can be attributed to the controlled increase in the Ru particle size. The co-presence of H_2 and O_2 is essential for controlling the Ru particle size accurately. In particular, an activated commercial 5 wt.% Ru/Al_2O_3 catalyst can reduce the high inlet CO concentration to be less than 10 ppm at low temperatures (350–385 K) even in the presence of H_2O and CO_2.

Acknowledgements

This research was supported by the Priority Research Centers Program through the National Research Foundation of Korea (NRF) funded by the Ministry of Education, Science, and Technology (2010-0029617). Experiments at PLS were supported in part by a Korea Research Foundation Grant funded by the Korean Government (MEST) (KRF-2007-412-J04001) and POSTECH. This work was completed with Ajou University research fellowship of 2010 (S-2010-G0001-00059).

Appendix A. Supplementary data

Supplementary data associated with this article can be found, in the online version, at http://dx.doi.org/10.1016/j.apcatb.2012.08.010.

References

[1] P. Poizot, S. Laruelle, S. Grugeon, L. Dupont, J.-M. Tarascon, Nature 407 (2000) 496–499.
[2] R. Makiura, T. Yonemura, T. Yamada, M. Yamauchi, R. Ikeda, Nature Materials 8 (2009) 476–480.
[3] J.A. Rodriguez, S. Ma, P. Liu, H. Hrbek, J. Evans, M. Pérez, Science 318 (2007) 1757–1760.
[4] S. Crossley, J. Faria, M. Shen, D.E. Resasco, Science 327 (2010) 68–72.
[5] Y. Zhai, D. Pierre, R. Si, W. Deng, P. Ferrin, A.U. Nilekar, G. Peng, J.A. Herron, D.C. Bell, H. Saltsburg, M. Mavrikakis, M. Flytzani-Stephanopoulos, Science 329 (2010) 1633–1636.
[6] J. Kim, J.E. Lee, J. Lee, Y. Jang, S.-W. Kim, K. An, J.H. Yu, T. Hyeon, Angewandte Chemie International Edition 45 (2006) 4789–4793.
[7] A.T. Bell, Science 299 (2003) 1688–1691.
[8] R. Schlögl, S.B.A. Hamid, Angewandte Chemie International Edition 43 (2004) 1628–1637.
[9] C.-X. Xiao, Z.-P. Cai, T.W. Wang, Y. Kou, N. Yan, Angewandte Chemie International Edition 47 (2008) 746–749.
[10] J. Kim, Y. Piao, N. Lee, Y.I. Park, I.-H. Lee, J.-H. Lee, S.R. Paik, T. Hyeon, Advanced Materials 22 (2009) 57–60.
[11] S.H. Joo, J.Y. Park, J.R. Renzas, D.R. Butcher, W. Huang, G.A. Somorjai, Nano Letters 10 (2010) 2709–2713.
[12] J.R.A. Sietsma, J.D. Meeldijk, J.P. den Breejen, M. Versluijs-Helder, A.J. van Dillen, P.E. de Jongh, K.P. de Jong, Angewandte Chemie International Edition 46 (2007) 4547–4549.
[13] G.L. Bezemer, J.H. Bitter, H.P.C.E. Kuipers, H. Oosterbeek, J.E. Holewijn, X. Xu, F. Kapteijn, A.J. van Dillen, K.P. de Jong, Journal of the American Chemical Society 128 (2006) 3956–3964.
[14] I.H. Son, M. Shamsuzzoha, A.M. Lane, Journal of Catalysis 210 (2002) 460–465.
[15] R. Farrauto, S. Hwang, L. Shore, W. Ruettinger, J. Lampert, T. Giroux, Y. Liu, O. Ilinich, Annual Review of Material Research 33 (2003) 1–27.
[16] E.D. Park, D. Lee, H.C. Lee, Catalysis Today 139 (2009) 280–290.
[17] E.-Y. Ko, E.D. Park, H.C. Lee, D. Lee, S. Kim, Angewandte Chemie International Edition 46 (2007) 734–737.
[18] S. Alayoglu, A.U. Nilekar, M. Mavrikakis, B. Eichhorn, Nature Materials 7 (2008) 333–338.
[19] A.U. Nilekar, S. Alayoglu, B. Eichhorn, M. Mavrikakis, Journal of the American Chemical Society 132 (2010) 7418–7428.
[20] Q. Fu, W.-X. Li, Y. Yao, H. Liu, H.-Y. Su, D. Ma, X.-K. Gu, L. Chen, Z. Wang, H. Zhang, B. Wang, X. Bao, Science 328 (2010) 1141–1144.
[21] B. Qiao, A. Wang, X. Yang, L.F. Allard, Z. Jiang, Y. Cui, J. Liu, J. Li, T. Zhang, Nature Chemistry 3 (2011) 634–641.
[22] S.H. Oh, R.M. Sinkevitch, Journal of Catalysis 142 (1993) 254–262.
[23] Y.H. Kim, E.D. Park, H.C. Lee, D. Lee, K.H. Lee, Catalysis Today 146 (2009) 253–259.
[24] G. Avgouropoulos, T. Ioannides, H. Matralis, Applied Catalysis B: Environmental 56 (2005) 87–93.
[25] C.R. Jung, A. Kundu, S.W. Nam, H.-I. Lee, Applied Catalysis B: Environmental 84 (2008) 426–432.
[26] B. Qiao, A. Wang, J. Lin, D. Su, T. Zhang, Applied Catalysis B: Environmental 105 (2011) 103–110.
[27] Z.K. Zhao, R.H. Jin, T. Bao, X.L. Lin, G.R. Wang, Applied Catalysis B: Environmental 110 (2011) 154–163.
[28] Q. Zhang, X. Liu, W. Fan, Y. Wang, Applied Catalysis B: Environmental 102 (2011) 207–214.
[29] A. Wörner, C. Friedrich, R. Tamme, Applied Catalysis A-General 245 (2003) 1–14.
[30] S.Y. Chin, O.S. Alexeev, M.D. Amiridis, Applied Catalysis A-General 286 (2005) 157–166.
[31] M. Echigo, T. Tabata, Applied Catalysis A-General 251 (2003) 157–166.
[32] Y.-F. Han, M. Kinne, R.J. Behm, Applied Catalysis B: Environmental 52 (2004) 123–134.
[33] Y.H. Kim, E.D. Park, H.C. Lee, D. Lee, Applied Catalysis A-General 366 (2009) 363–369.
[34] Y.H. Kim, E.D. Park, Applied Catalysis B: Environmental 96 (2010) 41–50.
[35] Y.H. Kim, S.-D. Yim, E.D. Park, Catalysis Today 185 (2012) 143–150.
[36] A.Y. Rozovskii, G.I. Lin, M.A. Kipnis, P.V. Samokhin, E.A. Volnina, I.A. Belostotsky, G.M. Grafova, I.N. Zavalishin, Topics in Catalysis 42-43 (2007) 437–441.
[37] A.Y. Rozovskii, M.A. Kipnis, E.A. Volnina, P.V. Samokhin, G.I. Lin, Kinetics and Catalysis 49 (2008) 92–102.
[38] A.Y. Rozovskii, M.A. Kipnis, E.A. Volnina, P.V. Samokhin, G.I. Lin, M.A. Kukina, Kinetics and Catalysis 50 (2009) 691–704.
[39] I. Rosso, M. Antonini, C. Galletti, G. Saracco, V. Specchia, Topics in Catalysis 30–31 (2004) 475–480.
[40] H.-F. Han, M.J. Kahlich, M. Kinne, R.J. Behm, Applied Catalysis B: Environmental 50 (2004) 209–218.
[41] H.-F. Han, M.J. Kahlich, M. Kinne, R.J. Behm, Physical Chemistry Chemical Physics 4 (2002) 389–397.
[42] G. Xu, Z.-G. Zhang, Journal of Power Sources 157 (2006) 64–77.
[43] M. Kipnis, E. Volnina, Applied Catalysis B: Environmental 98 (2010) 193–203.
[44] B. Ravel, M. Newville, Journal Synchrotron Radiation 12 (2005) 537–541.
[45] K. Pirkkalainen, R. Serimaa, Journal of Applied Crystallography 42 (2009) 442–447.
[46] J. Aßmann, D. Crihan, M. Knapp, E. Lundgren, E. Löffler, M. Muhler, V. Narkhede, H. Over, M. Schmid, A.P. Seitsonen, P. Varga, Angewandte Chemie International Edition 44 (2005) 917–920.